Transactions, SMiRT-23
Manchester, United Kingdom - August 10-14, 2015
Division I, Paper ID 180 (Mechanics of Materials)

Prediction and Validation of Multi-axial Stress State Effects on Creep Failure of Pre-Compressed 316H Stainless Steel

Mohammed-Rafi Riley[1], Ali Mehmanparest[2] and Catrin Davies[3]

[1] Research Postgraduate, Imperial College London, UK
[2] Lecturer, Cranfield University, UK
[3] Lecturer, Imperial College London, UK

ABSTRACT

The introduction of plastic pre-strain in reactor plant components, through various fabrication processes, has shown to reduce creep rupture life and creep ductility. This work investigates the effects of compressive pre-strain on the creep life of 316H stainless steel under multiaxial stress states through the use of notched bar specimens with two notch acuities. Tests were carried out at 550°C to simulate conditions existing within high temperature power plants. Similar results to that found from previous testing of this type on non-pre-compressed material was seen, suggesting material pre-compression has minimal influence on stress triaxiality. A notch strengthening effect occurs with a notch strengthening factor (NSF) of approximately 1.13 for this pre-compressed material. Results were validated against the Cocks and Ashby failure model which found that the model under predicts the effect of stress triaxiality. Post-test metallography show results as expected with damage visible at the locations of high stress triaxiality predicted using finite element modelling.

INTRODUCTION

Following fabrication processes such as pipe bending or welding significant plastic strain can exist in plant components which operate under multi-axial stress states (Bray, Dennis, & Bradford, 2010). The influence of plastic pre-strain to 4, 8 and 12 %, introduced in compression at room temperature, on the uniaxial creep deformation and crack growth behaviour of 316H stainless steel has recently been examined Ainsworth, (2013), Amouzouvi (1986), Liaw & Landes (1986), Mehmanparast et. al (2013), Mehmanparast et. al, (2014), Minami & Arimochi (2001), Sivaprasad et. al (2000). Prior plastic pre-strain has been found to reduce the creep rupture life and creep ductility of the material in addition to accelerating the creep crack growth rates. To understand the multi-axial behaviour of pre-strained material notch bar tests with a range of notch acuities are required, the results of which can also be used to validate creep failure models.

In this work, preliminary results on the failure behaviour of relatively sharp and blunt notched bar creep tests are reported. The results have been used to validate the Cocks and Ashby, Ashby & Cocks (1980) model to predict creep failure under triaxial stress states. Post-test metallography has also been performed to examine the damage distribution in the vicinity of the notch.

MATERIAL

The 316H SS used in this analysis was provided by EDF Energy and taken from a service exposed steam header (Header 1B1/1, Cast 53415 taken from Heysham 1 station), previously denoted Header A (Mehmanparest, 2010). Header A was in service for 87790 hours at an operating temperature of 523°C. The header component was heat treated, after removal, for three hours at 1050 °C and then water quenched.

Blocks of approximately 63 x 26 mm in cross-section, taken from Header A, were uniformly pre-compressed (PC) to 8 % true plastic strain at room temperature. The pre-compression was performed along

the axial direction of the header component. Uniaxial and notched bar specimens have been extracted from the pre-strained blocks with the specimen loading direction parallel to the pre-compression axis.

EXPERIMENTAL PROCEDURE

The test geometry is detailed in Figure 1(a). The insets in Figure 1(a) show the relatively blunt and sharp notch geometries with net diameter to notch radii ratios of a/R = 1.5 and a/R = 2.4, respectively. Testing was performed according to the code of practice guidelines set out in, Webster et al. (2004) however an advanced diametric expansion gauge was developed and employed in this work that enabled in-situ measurements of the sample's notch diameter to be obtained, as shown in Figure 1(b). To measure the axial displacement of the sample, capacitance gauges were employed which were located inside the furnace as shown in Figure 1(b). Capacitance gauges provide a more local measurement than LVDTs which have to be located outside the furnace and connected to the samples via an additional extensometer. Three blunt and three sharp notched geometries have been tested to date. All samples were tested at 550 °C and were loaded to a stress that would lead to practical test durations, as detailed in Table 1.

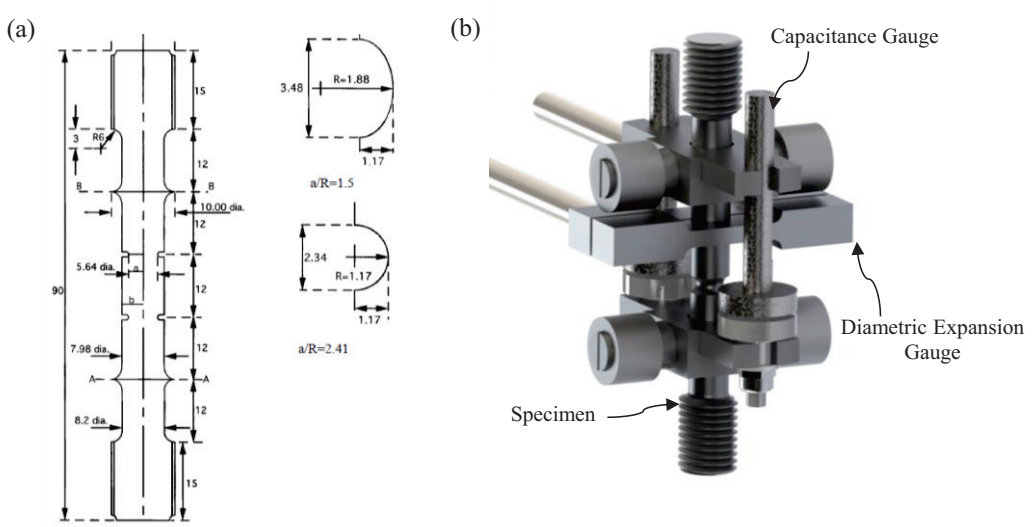

Figure 1 : (a) Engineering drawing of the notched bar specimens with insets of the notch geometry (b) illustration of the test assembly

Table 1: Test matrix

Test piece ID	a/R	Net stress (σ_{net} , MPa)
B5	1.50	390
B7	1.50	375
B8	1.50	410
S1	2.14	387
S2	2.14	330
S3	2.14	380

STRESS DISTRIBUTIONS IN A NOTCHED BAR

To accurately investigate the effect of stress tri-axiality on the creep properties of the material, an understanding of the stress fields across the notched bar is required. Finite element models have been used to calculate these distributions.

Finite Element Model

A finite element model of both notched bar geometries was developed. Exploiting the symmetry and axi-symmetry of the specimen geometry, only a quarter of the specimen was modelled using 2D four-node axisymmetric elements (CAX4). A fine mesh with smallest element size ahead of the notch root of 0.046 mm x 0.050 mm was applied around the notch root which was increased to 0.102 mm x 0.100 mm out of the notch region. The tensile, average creep strain rate properties and creep ductility used in the analysis are summarised in Table 2, which were taken from Mehmanparast et al. (2013).

Table 2: Material Properties

Yield Stress, σ_y	259 MPa	Power Law constant. A_A	1.42×10^{-39}
Youngs Modulus	140 GPa	Power law exponent, n_A	14.3
Poissons Ratio	0.3	Creep Ductility, ε_f	13.6 %

Notch Throat Stress Distribution

Figure 2 shows the distributions of the von-Mises (σ_e) and maximum principle stress (σ_1) across the notch throat at steady state creep conditions where *r* is the distance from the central axis of the specimen (i.e. *r/a* = 0 is at the centre of the specimen and *r/a* =1 at the notch surface). The maximum σ_1 occurs below the notch surface at *r/a* values of approximately 0.7 and 0.5 for the sharp and blunt notch, respectively. For both notch acuities σ_e is maximum at the notch surface.

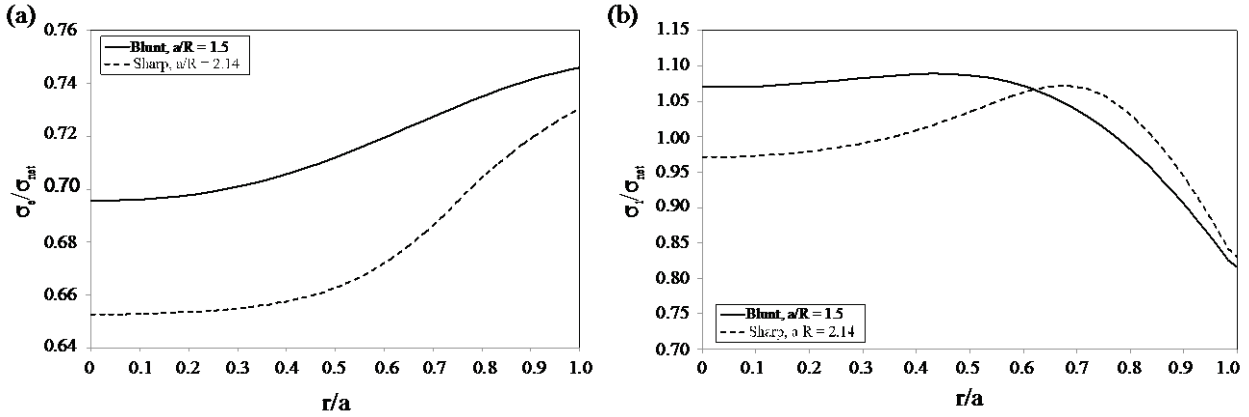

Figure 2 : (a) Mises equivalent and (b) maximum principle stress distribution across the throat area for steady state creep conditions.

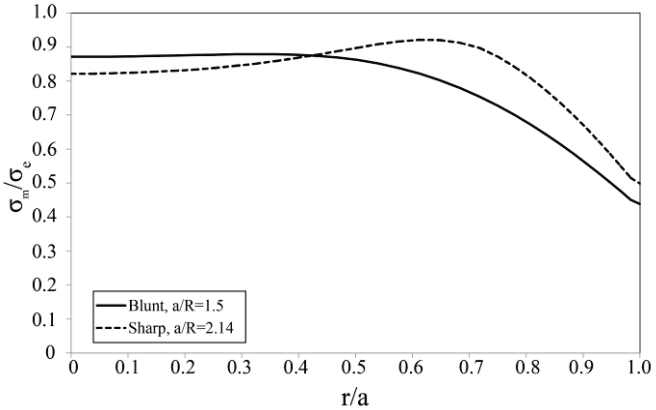

Figure 3: Graphs of tri axiality across the notch throat for (a) n=14 (b) n=5

The triaxiality across the throat is shown in Figure 3. The sharper notch has generally higher values of triaxiality, as expected, with a peak value of around 9.3 which is approximately 6% higher than that of the blunt notch. As detailed in Bettinson (2001), Nikbin et al. (2004) the peak triaxiality ratio increases with an increase in notch acuity and tends closer to the notch surface. Maximum ratios of σ_m/σ_e for the blunt and sharp notch are seen at r/a values of approximately 0.4 and 0.65, respectively.

Skeletal Points

It has been shown in Webster et al. (2004) that an approximate skeletal point can be identified where the stress state (i.e. σ_m, σ_e and σ_1) is insensitive to creep exponent (n). This point can be used to characterise the creep behaviour of a notched bar for a given net section stress, (σ_{net}). Once the skeletal stresses are known, the creep deformation of a notched bar can be analysed without any need for further numerical analysis. The skeletal points of various notch bars with different notch acuities have been reported in (Nikbin et al., 2004). In addition to this, FE analysis have been performed for the two notch geometries considered here and the results of the skeletal stresses, normalised by σ_{net} , are shown in Table 3 .

Table 3: Table showing the skeletal stress ratios for a/R=1.5 and 2.14

a/R	$\sigma_m^{sk}/\sigma_{net}$	$\sigma_e^{sk}/\sigma_{net}$	$\sigma_1^{sk}/\sigma_{net}$
1.5	0.70	0.54	1.04
2.14	0.67	0.60	1.10

CREEP DATA ANALYSIS

Creep Failure Analysis

A true failure strain (ε_f^{ROA}) can be determined through measuring the diameter of the un-failed notch directly after load-up (d_{load}) and after failure (d_f) using Equation 6.

$$\varepsilon_f^{ROA} = 2\ln\left(d_f / d_{load}\right) \tag{1}$$

Difficulties were initially encountered in monitoring the in-situ notch diametric expansion. This lead to difficulties in measuring, d_{load} and hence determining an accurate ε_f^{ROA}. However, it may be assumed can be made such that d_{load} is equal to the initial untested notch diameter (d_0), suggesting that the reduction in area of the notch is negligible during load up. This assumption is deemed acceptable given the findings from literature Mehmanparest (2010), where it states that the influence of pre-compression may almost eliminate the plastic strain during load up. This assumption was further deemed feasible after FE analysis predicted the strain at load up to be small (~0.03%).

Equivalent Stress Criterion

In a number of materials including austenitic stainless steel, the creep-rupture mechanism is found to be related to a combination of the maximum principal and equivalent stresses Hayhurst (1972). This stress combination is here referred to as the rupture controlling stress, σ_{RC}, and is expressed as

$$\sigma_{RC} = \alpha_{RC}\sigma_1 + \left(1-\alpha_{RC}\right)\bar{\sigma} \tag{2}$$

where σ_{RC} is material parameter determined from sets of creep tests on notched specimens, carried out under different multiaxial stress states ($0 \le \sigma_{RC} \le 1$). As shown in Figure 2 the maximum value of principle stress is just below the notch root. If failure initiates here then damage will accumulate ahead of the notch

root and failure will involve the linking of this damage to the notch surface. Similarly for σ_{RC} control, the damage is predicted to occur first at the surface of the notch root where the von-Mises stress is maximum.

COMPARISON OF UNIAXIAL AN NOTCH BAR CREEP DATA

The rupture data for all notched bar tests are given in Table 4 and plotted in Figure 4 and compared to that of uniaxial data taken from Mehmanparest (2010) . A single trend line is fitted to the notch data set and a separate line fitted to the uniaxial data set. A notch strengthening effect occurs with a notch strengthening factor (NSF) of approximately 1.13 for this 8% pre-compressed material. This NSF is similar to that found on as-received material (≈1.09) Bettinson (2001), suggesting that the introduction of a notch in a material may have the same effect on a specimen independent of material pre-compression.

Table 4: Failure properties of notched bar tests

Test piece ID	a/R	Net section stress (σ_{net} , MPa)	t_r (hours)	ε_f^{ROA} (%)
B5	1.50	390	394	0.96
B7	1.50	375	503	3.90
B8	1.50	410	438	0.88
S1	2.14	387	391	1.05
S2	2.14	330	1400	1.70
S3	2.14	380	358	2.00

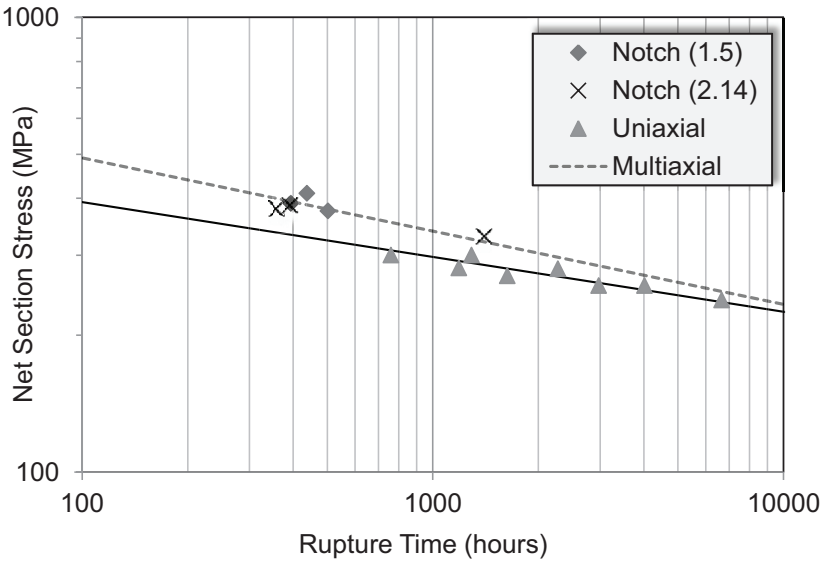

Figure 4: Comparison of the stress rupture data from uniaxial and notch bar samples

To calculate σ_{RC}, the values of σ_e and σ_1 were analysed at a single point. Use was made of the skeletal stress ratios from Table 3 such that values can be attained for the skeletal points for both notch acuities, and are shown in Figure 5 and 6. It is apparent from these figures that neither σ_e or σ_1 accurately capture the rupture data. However, a value of $\sigma_{RC} = 0.45$ provides a good fit to the data, suggesting that an almost equal dependency of von-Mises and maximum principle stress govern the rupture behaviour of the material, with a slightly higher dependency on the von-Mises stress. This value is almost identical to that of as-received material ($\alpha_{RC} = 0.47$) Bettinson (2001). A plot of the rupture controlling stress with rupture time is given in Figure 7.

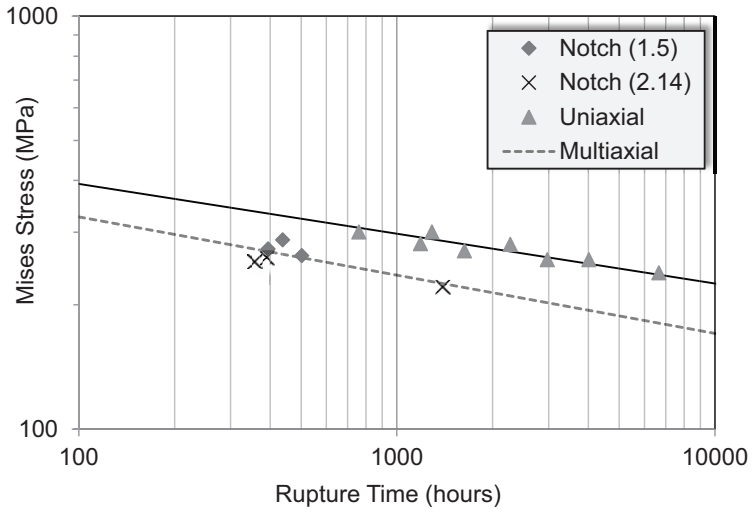

Figure 5: Rupture life at the skeletal points based on Mises stress

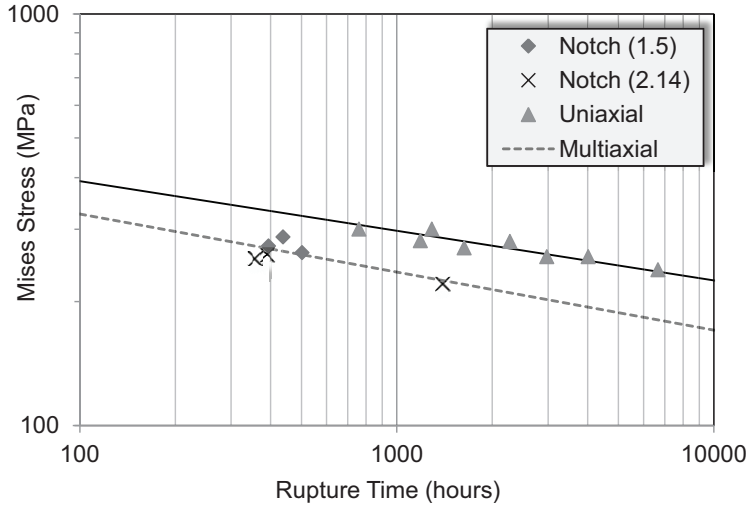

Figure 6: Rupture life at the skeletal points based on max. principle stress

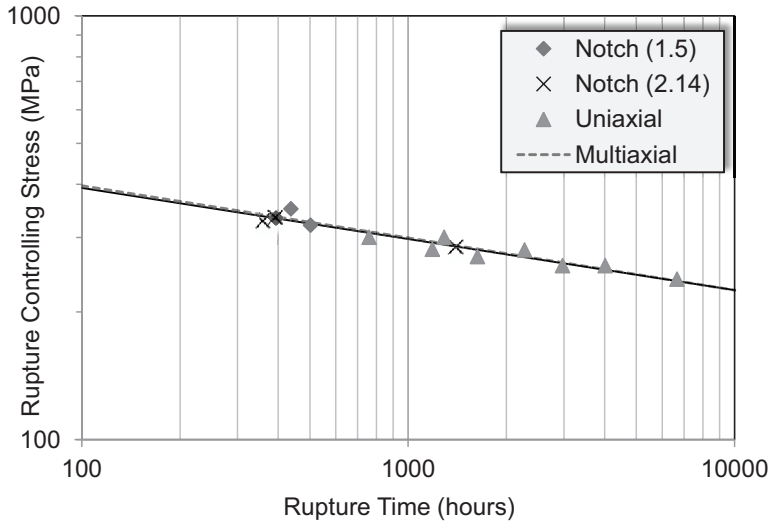

Figure 7: Rupture life based on a rupture controlling stress

Influence on Stress Tri-axiality on Creep Ductility

Under multiaxial stress conditions the failure strain, denoted ε_f^*, may be estimated from the uniaxial failure strain ε_f using a multiaxial strain factor (*MSF*) such as

$$\varepsilon_f^* = MSF\,\varepsilon_f = \varepsilon_f \sinh\left[\frac{2}{3}\left(\frac{n-1/2}{n+1/2}\right)\right] \Big/ \sinh\left[2h\left(\frac{n-1/2}{n+1/2}\right)\right] \tag{3}$$

which has been based on the Cocks and Ashby void growth model Ashby & Cocks (1980) . Using the stresses at the skeletal points, the dependence on creep ductility has been predicted using the Cocks and Ashby model and compared to values obtained through testing. The failure strain values are, ε_f =13.6 % for uniaxial tests Mehmanparast et al. (2013) and it is assumed that the values of, ε_f^{ROA} are equal to ε_f^*. This is an estimate given the difficulties of attaining an exact value of ε_f^{ROA} at the skeletal points experimentally. Hence values from Table 4 are indicative of ε_f^*. A creep exponent of n = 14 has been used for the Cocks and Ashby model and the ductility ratio is evaluated based on the un-failed notch of the specimen. The results of this analysis are shown in Figure 8. It can be seen that the experimental data follow a similar trend to the model's predictions, though the model, and the assumption made, somewhat under predicts the effects of stress triaxiality.

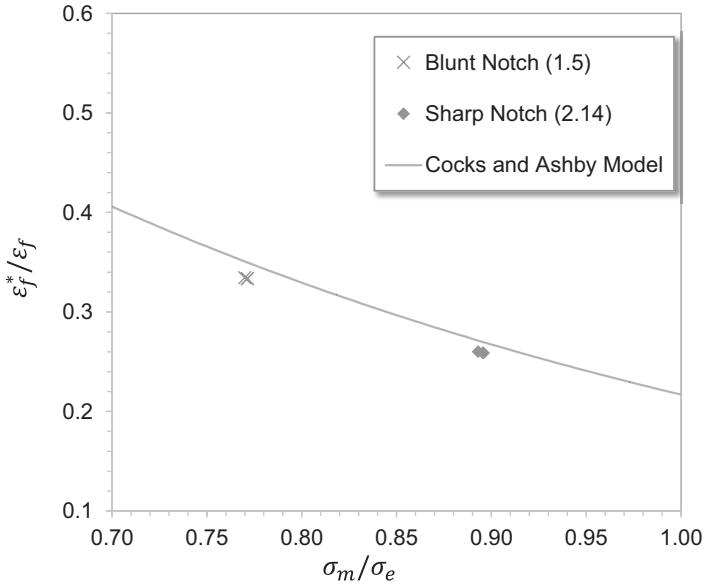

Figure 8: Failure strain dependence on tri-axiality for notched bars compared to model predictions

METALLOGRAPHY

To examine the influence of pre-compression on the materials microstructure, metallographic analysis was performed around the vicinity of the notch after specimen failure. Figure 9 shows the section through the un-failed notch for the sharp notched bar (σ_{net} = 330 MPa). Creep damage in the form of inter-granular micro-cracks can be seen across the notch throat, with damage occurring closer to the notch root for the sharper notch than for that of a blunt notched bar Figure 10 (σ_{net} = 375 MPa). This is expected given the stress triaxiality maxima locations. Similar results are seen of metallographic analyses on notched bars in [8].

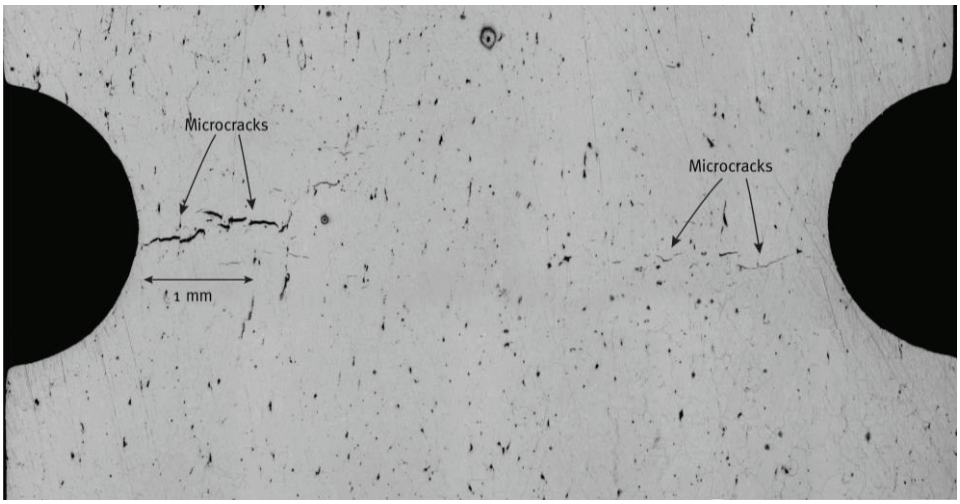

Figure 9: Throat cross section for the sharp notched sample at σ_{net} = 375 MPa

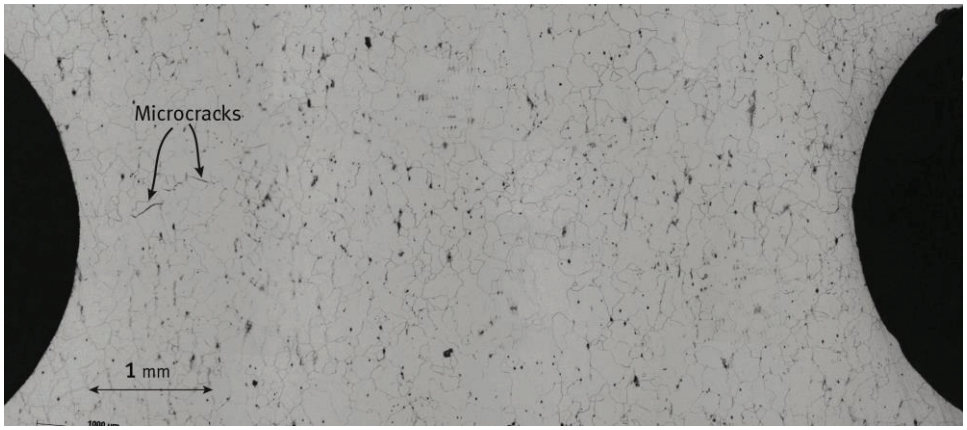

Figure 10: Throat section for blunt notched sample at σ_{net} = 375 MPa

The failed notch profile for the same sharp and blunt notched bar is shown in Figure 11 and 12, respectively. The fracture surface lies in a plane close to the centre of the notch and is normal to the applied stress. Both profiles for the sharp and blunt notched bars show predominately regions of inter-granular crack growth.

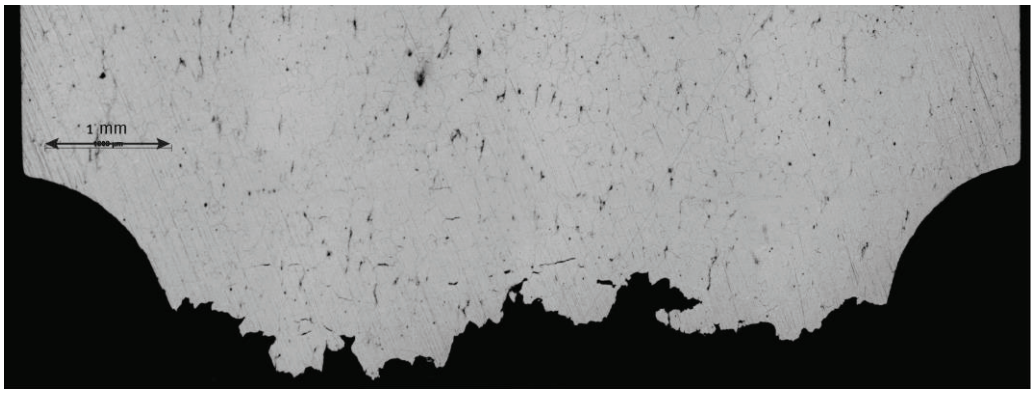

Figure 11: Fracture surface for the sharp notched sample

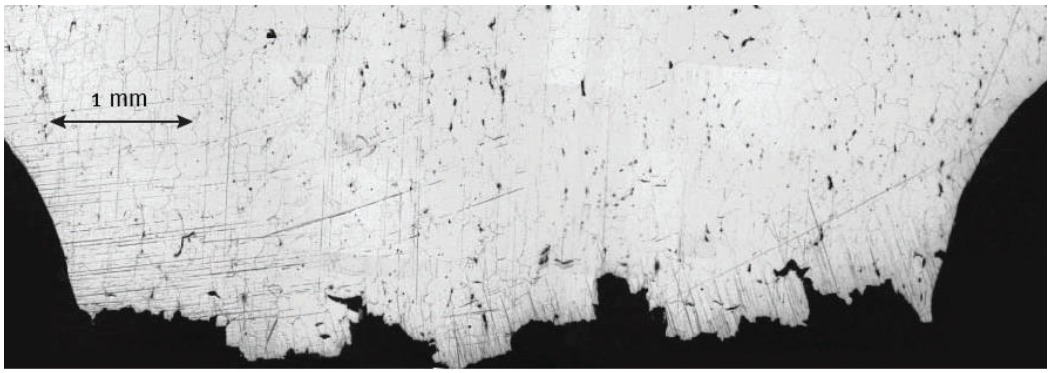

Figure 12: Fracture surface for the blunt notched sample

CONCLUSION

Creep rupture tests were performed on a total of six notched bar samples, (three sharp notched and three blunt notched). Little variation was seen between the rupture data of the two notch acuities, this can be attributed to the small difference in peak stress triaxiality value between both specimens. The NSF was found to be almost equal to that of previous work on non-pre-compressed material, suggesting that material pre-compression has minimal influence on NSF. Validation of the results against the Cocks and Ashby model showed that the model under predicts the effects of stress triaxiality, though the results do seem to follow the models trent. Initial FE modelling allowed the prediction of damage locations which were later validated through post-test metallography. Future work intends to concentrate on developing the FE model further to allow full creep damage simulation with the implementation of various creep damage models. More notched bar tests will also be performed concentrating on longer creep rupture times than those performed to date. In conclusion, with the data received to date, it seems that material pre-compression has minimal effect when under multiaxial stress states and exhibits behaviour similar to that of non-pre-compressed material. This is proven by the similar NSF and α_{RC} values.

REFERENCES

Ainsworth, R. A. (2013). An assessment of the effects of prestrain on upper shelf fracture toughness, *21*(4), 219–224.

Amouzouvi, K. F. (1986). A comparative fracture study of a slightly prestrained low alloy steel and a slightly prestrained austenitic stainless steel. *Materials Science and Engineering*, *78*(1), 65–70. http://doi.org/http://dx.doi.org/10.1016/0025-5416(86)90080-7

Ashby, M. F., & Cocks, A. C. F. (1980). Intergranular fracture during power-law creep under multi-axial stress. *Metal Science*, *14*, 395–402.

Bettinson, A. (2001). *The influence of constraint on the creep crack growth of 316H stainless steel*. Imperial College London.

Bray, D., Dennis, R., & Bradford, R. (2010). Modelling the complex manufacturing history of a pipework joint and assessment of its through life creep-fatigue damage using finite element based methods. In *ASME 2010 Pressure Vessels & Piping Division / K-PVP Conference*.

Hayhurst, D. R. (1972). Creep rupture under multiaxial states of stress. *J. Mech. Phys. Solids*, *20*, 381–390.

Liaw, P. K., & Landes, J. D. (1986). Influence of prestrain history on fracture toughness properties of steels. *Metallurgical Transactions A*, *17*(3), 473–489. Retrieved from http://www.scopus.com/inward/record.url?eid=2-s2.0-0022677691&partnerID=40&md5=9620a496afa515a35aa7748f9d81a82e

Mehmanparast, A., Davies, C. M., Dean, D. W., & Nikbin, K. M. (2013). The influence of pre-compression on the creep deformation and failure behaviour of Type 316H stainless steel. *Engineering Fracture Mechanics*, *110*(0), 52–67. http://doi.org/http://dx.doi.org/10.1016/j.engfracmech.2013.08.006

Mehmanparast, A., Davies, C. M., Dean, D. W., & Nikbin, K. M. (2014). Plastic pre-compression and creep damage effects on the fracture toughness behaviour of Type 316H stainless steel. *Engineering Fracture Mechanics*, *131*(0), 26–37. http://doi.org/http://dx.doi.org/10.1016/j.engfracmech.2014.10.005

Mehmanparest, A. (2010). *The influence of inelastic damage on creep, fatigue and fracture toughness*. Imperial College London.

Minami, F., & Arimochi, K. (2001). Evaluation of prestraining and dynamic loading effects on the fracture toughness of structural steels by the local approach. *Journal of Pressure Vessel Technology, Transactions of the ASME*, *123*(3), 362–372. Retrieved from http://www.scopus.com/inward/record.url?eid=2-s2.0-0001106196&partnerID=40&md5=4beee7ce24c653f29fd7b4bab715e85b

Nikbin, K., Webster, G., & Biglari, F. (2004). Finite element analysis of notched bar skeletal point stresses and dimension changes due to creep. *Fatigue Fracture of Engineering Materials Structures*.

Sivaprasad, S., Tarafder, S., Ranganath, V. R., & Ray, K. K. (2000). Effect of prestrain on fracture toughness of HSLA steels. *Materials Science and Engineering: A*, *284*(1–2), 195–201. http://doi.org/http://dx.doi.org/10.1016/S0921-5093(00)00739-5

Webster, G. A., Holdsworth, S. R., & Loveday, M. S. (2004). A code of practice for conducting notched bar creep tests and for interpreting data. High Temperature Mechanical Testing Committee.